Rapid Communications

Dropping an impurity into a Chern insulator: A polaron view on topological matter

A. Camacho-Guardian,[1] N. Goldman,[2] P. Massignan,[3] and G. M. Bruun[1]

[1]*Department of Physics and Astronomy, Aarhus University, Ny Munkegade, DK-8000 Aarhus C, Denmark*

[2]*Center for Nonlinear Phenomena and Complex Systems, Université Libre de Bruxelles, CP 231, Campus Plaine, B-1050 Brussels, Belgium*

[3]*Departament de Física, Universitat Politècnica de Catalunya, Campus Nord B4-B5, E-08034 Barcelona, Spain*

(Received 1 November 2018; revised manuscript received 25 January 2019; published 5 February 2019)

We investigate the properties of an impurity particle interacting with a Fermi gas in a Chern-insulating state. The interaction leads to the formation of an exotic polaron, which consists of a coherent superposition of the topologically trivial impurity and the surrounding topological cloud. We characterize this intriguing topologically composite object by calculating its transverse (Hall) conductivity, using diagrammatic as well as variational methods. The "polaronic Hall conductivity," i.e., the transverse drag exerted by the dressing cloud on the impurity, is shown to exhibit a sharp jump from zero to a finite value whenever the surrounding cloud enters a topologically nontrivial state. In this way, the polaron partially inherits the topological properties of the Chern insulator through genuine interaction effects. This is also analyzed at the microscopic level of wave functions, by identifying a "composite Berry curvature" for the polaron, which closely mimics the Berry curvature of the Chern insulator's band structure. Finally, we discuss how this interplay between topology and many-body correlations can be studied in cold-atom experiments, using available technologies.

DOI: 10.1103/PhysRevB.99.081105

Introduction. The exploration of topological states of matter constitutes one of the most active fields in condensed-matter physics [1–3]. In parallel to the identification of novel topological properties in single-particle band structures [4–6], intense efforts are dedicated to the rich interplay of topological bands and interparticle interactions [7–20]. In addition to condensed-matter systems, topological band structures have also been studied in the context of ultracold gases [21–23]. These atomic systems are particularly well suited to investigate the role of interactions in topological phases [24–30], since the interaction strength between neutral atoms can be easily tuned experimentally [31]. This feature of cold-atom systems has led to various fundamental discoveries [32–34]; in particular, ultracold gases have deepened our understanding of how mobile impurities behave within ultracold Fermi [35–38] or Bose [39,40] gases.

Here, we show that impurity physics provides a promising framework to explore interacting topological systems in a realistic and controlled setting. Specifically, we consider an impurity moving in a honeycomb lattice and interacting with a gas of "majority" particles forming a Chern insulator. The interaction leads to the formation of a polaron consisting of a (topologically trivial) impurity dressed by a cloud of majority particles forming a topological phase. Using both a diagrammatic and a variational approach, we calculate the transverse (Hall) conductivity of this intriguing composite object, and show that it partially reflects the Hall-type properties of the majority particles. Physically, this is due to the drag exerted by the dressing cloud on the impurity, and it is thus a genuine interaction effect. At the microscopic level, we identify a "composite Berry curvature" for the polaron and show that it closely mimics the Berry curvature of the underlying Chern insulator's band structure. Our developments are reminiscent of a recently proposed interferometric scheme, which involves mobile impurities bound to quasiparticles in fractional quantum Hall states [41].

System. Consider a mobile impurity, denoted as a $\downarrow$ particle, immersed in a gas of fermionic majority (spin $\uparrow$) particles. Both the impurity and the majority particles reside in a honeycomb lattice with nearest-neighbor hopping. In addition, the majority particles experience next-nearest-neighbor hopping, which breaks time-reversal symmetry, and a broken inversion symmetry given by an energy offset between neighboring sites [see Fig. 1(a)]. Thus, the Hamiltonian for the impurity corresponds to the usual nearest-neighbor tight-binding model for graphene [42], whereas the Hamiltonian for the majority particles corresponds to the Haldane model [43],

$$\hat{H}_0 = -t_1 \sum_{\sigma=\uparrow,\downarrow} \sum_{\langle i,j\rangle} \hat{c}^\dagger_{iA\sigma}\hat{c}_{jB\sigma} - t_2 \sum_{\langle\langle i,j\rangle\rangle} e^{i\phi_{ij}}\hat{c}^\dagger_{iA\uparrow}\hat{c}_{jB\uparrow} + \text{H.c.} + \Delta \sum_i \left(\hat{c}^\dagger_{iA\uparrow}\hat{c}_{iA\uparrow} - \hat{c}^\dagger_{iB\uparrow}\hat{c}_{iB\uparrow}\right) = \sum_{\mathbf{k}\alpha\sigma} \varepsilon_{\sigma\alpha}(\mathbf{k})\hat{\gamma}^\dagger_{\mathbf{k}\alpha\sigma}\hat{\gamma}_{\mathbf{k}\alpha\sigma}. \tag{1}$$

Here, $\hat{c}^\dagger_{is\sigma}$ creates an impurity/majority particle for $\sigma = \downarrow, \uparrow$ on the $s = A/B$ site in unit cell i, and t_1 is the nearest-neighbor hopping matrix element, which is taken to be the same for both kinds of particles. In the Haldane model [43], the matrix elements for the next-nearest-neighbor hopping of the majority particles have strength t_2 and phase ϕ_{ij}; we have $\phi_{ij} = \phi$, or $\phi_{ij} = -\phi$, depending on whether the next-nearest hopping process is performed in a clockwise or anticlockwise fashion, respectively. The staggered sublattice potential Δ splits the energy of the A and B sites. The second line of Eq. (1) displays the diagonalized Hamiltonian, and introduces the operator $\hat{\gamma}^\dagger_{\mathbf{k}\alpha\sigma}$, which creates a particle in the single-particle eigenstate of the Haldane ($\sigma = \uparrow$) or graphene ($\sigma = \downarrow$) Hamiltonian, in

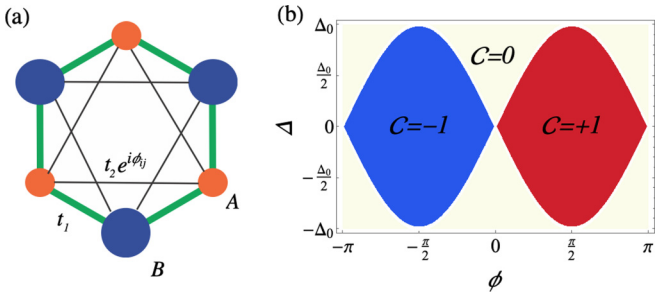

FIG. 1. (a) Both the impurity and majority particles live in a honeycomb lattice with nearest-neighbor hopping with strength t_1. The majority particles in addition experience next-nearest-neighbor hopping with strength t_2 and phase ϕ_{ij}, and an energy offset between the triangular sublattices of A and B sites. (b) The phase diagram of the Haldane insulator for the majority atoms. Here, $\Delta_0 = 3^{3/2}t_2$.

band $\alpha = (1, 2)$ and with quasimomentum $\mathbf{k}$ within the first Brillouin zone (BZ); the energy of this state is $\varepsilon_{\sigma\alpha}(\mathbf{k})$. In the following, we assume that the majority particles fill the lowest band completely in the absence of interactions so that they form a topological band insulator. The well-known topological phase diagram of the Haldane model, characterized by the Chern number $\mathcal{C}$, is shown in Fig. 1(b).

The impurity interacts with the majority particles via the contact potential

$$\begin{aligned}\hat{H}_{\text{int}} &= g\sum_i \sum_{s=A,B} \hat{c}^\dagger_{is\uparrow}\hat{c}^\dagger_{is\downarrow}\hat{c}_{is\downarrow}\hat{c}_{is\uparrow} \\ &= \frac{g}{N}\sum_{\substack{\mathbf{k}\mathbf{k}'\mathbf{q}\\ \alpha\beta\alpha'\beta'}} W^{\alpha\beta}_{\alpha'\beta'}(\mathbf{k},\mathbf{k}',\mathbf{q})\hat{\gamma}^\dagger_{\mathbf{k}+\mathbf{q}\alpha\uparrow}\hat{\gamma}^\dagger_{\mathbf{k}'-\mathbf{q}\alpha'\downarrow}\hat{\gamma}_{\mathbf{k}'\beta'\downarrow}\hat{\gamma}_{\mathbf{k}\beta\uparrow},\end{aligned} \tag{2}$$

where N is the number of unit cells in the lattice, and $W^{\alpha\beta}_{\alpha'\beta'}(\mathbf{k},\mathbf{k}',\mathbf{q})$ gives the strength of the scattering of a majority/impurity particle in band β/β' with momentum $\mathbf{k}/\mathbf{k}'$ into a majority/impurity particle in band α/α' with momentum $\mathbf{k}+\mathbf{q}/\mathbf{k}'-\mathbf{q}$. A detailed expression for $W^{\alpha\beta}_{\alpha'\beta'}(\mathbf{k},\mathbf{k}',\mathbf{q})$ is given in the Supplemental Material [44].

The polaron. The interaction $\hat{H}_{\text{int}}$ results in the creation of a quasiparticle called the Fermi polaron, which consists of the impurity "dressed" by a cloud of fermionic majority atoms. Such polarons have been studied intensely in the absence of a lattice using cold-atom systems [35–38,45]. The polaron ground-state wave function is well approximated by the so-called Chevy ansatz [46]

$$\begin{aligned}|\psi_0\rangle &= \left(\sqrt{Z_0} + \sum_{\mathbf{Q},\mathbf{q},\alpha} M_{\mathbf{Q},\mathbf{q},\alpha}\hat{\gamma}^\dagger_{\mathbf{q}2\uparrow}\hat{\gamma}^\dagger_{\mathbf{Q}-\mathbf{q}\alpha\downarrow}\hat{\gamma}_{\mathbf{Q}1\uparrow}\hat{\gamma}_{\mathbf{0}1\downarrow}\right)|\varphi_0\rangle \\ &\equiv \sqrt{Z_0}|\varphi_0\rangle + \sum_{\mathbf{Q},\mathbf{q},\alpha} M_{\mathbf{Q},\mathbf{q},\alpha}|\varphi_{\mathbf{Q},\mathbf{q},\alpha}\rangle,\end{aligned} \tag{3}$$

where Z_0 is the quasiparticle residue while $|\varphi_0\rangle$ and $|\varphi_{\mathbf{Q},\mathbf{q},\alpha}\rangle$ are the noninteracting ground and excited states, respectively. The coefficients $\sqrt{Z_0}$ and $M_{\mathbf{Q},\mathbf{q},\alpha}$ are obtained by minimizing $\langle\hat{H}_0 + \hat{H}_{\text{int}} - E\rangle$, as explained in the Supplemental Material [44]. The second term in Eq. (3) describes the dressing of the impurity by particle-hole excitations of the majority particles from the valence to the conduction band while exciting the impurity to band α. Since the Haldane bands have nontrivial topological properties for certain values of (ϕ, Δ), the polaron is a coherent mixture of a topologically trivial impurity surrounded by a topological dressing cloud of majority particles. This raises the fascinating question of whether the polaron inherits some the topological properties of its dressing cloud and how one can characterize this phenomenon. We stress that the polarons stem from the genuine interacting nature of our composite system, and that such objects cannot be realized by simply connecting two noninteracting layers through hopping.

External force and transverse current. We do not expect the topological properties of the polaron to be reflected in quantities such as its energy. Inspired by the famous Thouless-Kohmoto-Nightingale-den Nijs (TKNN) relation, linking the transverse (Hall) conductivity to the Chern number [47], we instead examine the transverse response of the polaron to an external force. The central question concerns the mechanism by which the quantized Hall response of the majority induces a polaronic Hall effect through interactions.

In order to measure the response of the polaron (and not that of the bare impurity only), we take the force $\mathbf{F}(\mathbf{r}) = -\nabla V(\mathbf{r})$ to act on both the impurity and the majority particles, i.e., on both components of the polaron. The perturbation corresponding to the force is then

$$\hat{H}'(t) = \int d^2 r V(\mathbf{r})\hat{\rho}(\mathbf{r}, t), \tag{4}$$

where $\hat{\rho} = \hat{\rho}_\uparrow + \hat{\rho}_\downarrow$ is the total density of the system. For concreteness, we consider a uniform force F_y in the y direction, i.e., $\mathbf{F}(\mathbf{r}) = -F_y\mathbf{e}_y$. The transverse Hall conductivity of the polaron σ^P_{xy} then determines the induced current density along the x direction, according to $\langle\hat{j}_{x\downarrow}\rangle = \sigma^P_{xy}\cdot(-F_y)$. The homogeneous current densities of the two components are given by the operators

$$\hat{\mathbf{j}}_\sigma = \frac{1}{N}\sum_{\mathbf{k}}\hat{\vec{\mathcal{J}}}(\mathbf{k}) = \frac{1}{N}\sum_{\mathbf{k}}\sum_{\alpha\beta}\hat{\gamma}^\dagger_{\mathbf{k}\beta\sigma}\vec{\mathcal{J}}_{\sigma\beta\alpha}(\mathbf{k})\hat{\gamma}_{\mathbf{k}\alpha\sigma}, \tag{5}$$

where the quantity $\vec{\mathcal{J}}_{\sigma\beta\alpha}(\mathbf{k})$, giving the current operator in the eigenbasis of the graphene and Haldane Hamiltonians, is given in the Supplemental Material [44].

The transverse current of the polaron due to the force Eq. (4) can be written in terms of the current-current correlation function within linear response. As shown in Ref. [44], we have

$$\sigma^P_{xy} = \lim_{\omega\to 0} -\frac{\mathcal{P}_{xy}(\omega)}{i\omega}, \tag{6}$$

where $\mathcal{P}_{xy}(\omega)$ is the Fourier transform of the current-current correlation function $\mathcal{P}_{xy}(t-t') = -iN\theta(t-t')\langle\psi_0|[\hat{j}_{x\downarrow}(t), \hat{j}_{y\uparrow}(t') + \hat{j}_{y\downarrow}(t')]|\psi_0\rangle$, with $\theta(t)$ the Heaviside function. As we will show below, the transverse conductivity in Eq. (6) encodes the topological properties of the impurity dressed by the topological cloud in Eq. (3). Besides, the longitudinal transport exhibits Bloch oscillations of the polaron [48].

Composite Berry curvature. The Berry curvature is an essential ingredient for understanding noninteracting Chern

insulators [1–3]. Likewise, the Lehmann representation can be used to express the transverse conductivity of the polaron in Eq. (6) as an integral over a "composite" Berry curvature, $\sigma^P_{xy} = \sum_{\mathbf{Q}} \mathcal{B}_{\downarrow\uparrow}(\mathbf{Q})$, where [44]

$$\mathcal{B}_{\sigma\sigma'}(\mathbf{Q}) = -i \sum_{\mathbf{k}_1,\mathbf{k}_2,\mathbf{q}} \sum_{\alpha,\beta,\alpha',\beta',\alpha''} \frac{\langle\psi_0|\hat{\mathcal{J}}^x_{\sigma\alpha\beta}(\mathbf{k}_1)|\psi_{\mathbf{Q},\mathbf{q},\alpha''}\rangle\langle\psi_{\mathbf{Q},\mathbf{q},\alpha''}|\hat{\mathcal{J}}^y_{\sigma'\alpha'\beta'}(\mathbf{k}_2)|\psi_0\rangle - x \leftrightarrow y}{(E_0 - E_{\mathbf{Q},\mathbf{q}})^2}. \tag{7}$$

Here, $|\psi_{\mathbf{Q},\mathbf{q},\alpha}\rangle$ is an interacting excited state of the polaron with energy $E_{\mathbf{Q},\mathbf{q}}$, which is adiabatically connected to the noninteracting excited state $|\varphi_{\mathbf{Q},\mathbf{q},\alpha}\rangle$ defined in Eq. (3). Importantly, the quantity $\mathcal{B}_{\sigma\sigma'}(\mathbf{Q})$, which describes the Berry curvature of an excitation involving spins σ and σ' with total momentum $\mathbf{Q}$, corresponds to the Berry curvature of the polaron in Eq. (3) when setting $\sigma = \uparrow$ and $\sigma' = \downarrow$. This new quantity emerges as a consequence of the combination of the many-body nature of the polaron and the underlying topological band structure of the majority particles. It is easy to show that $\mathcal{B}_{\uparrow\uparrow}(\mathbf{Q})$, on the other hand, recovers the usual expression for the Berry curvature of the Haldane model [44].

Diagrammatic analysis. We now use a diagrammatic analysis to calculate the transverse conductivity Eq. (6). This allows us to include the interaction in a systematic way using perturbation theory in the coupling strength g. The calculation is equivalent to using the many-body Chevy ansatz in Eq. (3) to evaluate the composite Berry curvature in Eq. (7) up to second order in g. The current-current correlation function is illustrated diagrammatically in Fig. 2. We assume zero temperature so that the polaron is initially in its ground state $|\psi_0\rangle$ with zero momentum. Since the Berry curvature vanishes for the energy bands of graphene, it follows that $\sigma^P_{xy} = 0$ when there are no interactions. The first-order diagrams also give no contribution to the transverse conductivity, as they correspond to a simple Hartree energy shift of the impurity energy. The first nonvanishing contribution to the transverse conductivity is therefore second order in g, and it is given by the diagrams shown in the lower panel of Fig. 2. They correspond to the contribution

$$\begin{aligned}\mathcal{P}_{xy}(\omega) = g^2 \sum_{k_1 k_2 k_3} \mathcal{J}^x_{\downarrow\beta'\alpha'}(\mathbf{k}_2)\mathcal{G}_{\downarrow\beta'}(k_2+\omega)\mathcal{G}_{\downarrow\alpha'}(k_2)\mathcal{G}_{\downarrow\kappa'}(k_3+k_2)\Big[W^{\beta\kappa}_{\kappa'\beta'}(\mathbf{k}_1+\mathbf{k}_3,\mathbf{k}_2,-\mathbf{k}_3)W^{\kappa\alpha}_{\alpha'\kappa'}(\mathbf{k}_1,\mathbf{k}_3+\mathbf{k}_2,\mathbf{k}_3)\mathcal{G}_{\uparrow\kappa}(k_1+k_3)\\ + W^{\beta\kappa}_{\alpha'\kappa'}(\mathbf{k}_1-\mathbf{k}_3,\mathbf{k}_3+\mathbf{k}_2,\mathbf{k}_3)W^{\kappa\alpha}_{\kappa'\beta'}(\mathbf{k}_1,\mathbf{k}_2,-\mathbf{k}_3)\mathcal{G}_{\uparrow\kappa}(k_1-k_3+\omega)\Big]\mathcal{G}_{\uparrow\alpha}(k_1)\mathcal{G}_{\uparrow\beta}(k_1+\omega)\mathcal{J}^y_{\uparrow\beta\alpha}(\mathbf{k}_1),\end{aligned} \tag{8}$$

where $\sum_k \equiv T\sum_{\omega_n}\sum_{\mathbf{k}}$ is a shorthand notation for a summation over a Matsubara frequency and integration over a two-dimensional (2D) momentum $\mathbf{k}$ inside the BZ, $k \equiv (\mathbf{k}, i\omega_n)$, and there is a summation over repeated band indices. The noninteracting Green's function for a σ particle in band α is $\mathcal{G}_{\sigma\alpha}(k)^{-1} = i\omega_n - \varepsilon_{\sigma\alpha}(\mathbf{k})$. In Ref. [44], we provide all first- and second-order diagrams for the current-current correlation function and evaluate the three Matsubara sums in Eq. (8) analytically. As usual, we add a positive infinitesimal part to the frequency ω to get the retarded correlation function $\mathcal{P}_{xy}(\omega)$.

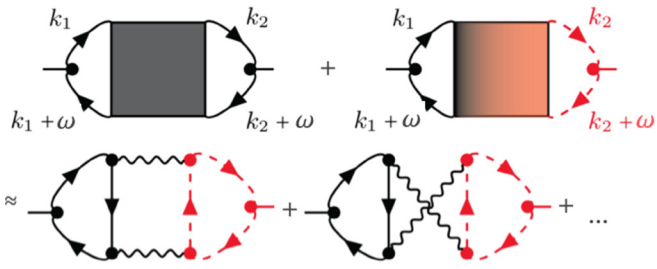

FIG. 2. Top: Diagrammatic representation of the transverse conductivity of the polaron. Bottom: Second-order nonzero diagrams. Black solid/red dashed lines denote the impurity/majority $\sigma = \downarrow, \uparrow$ Green's function and wavy lines the interaction.

Note that our second-order calculation is conserving [49], which is a major challenge for arbitrary interaction strengths [50].

The fact that the first nonzero contribution to the transverse conductivity is proportional to g^2 can be understood as follows. The transverse current of the polaron is caused by the drag exerted by its dressing cloud. This drag is proportional to the scattering rate between the impurity and the majority particles, which again is proportional to the scattering cross section scaling as g^2.

Results. We now discuss our main results shown in Figs. 3 and 4. The transverse conductivity of the ground-state polaron σ^P_{xy} is obtained by evaluating the diagrammatic expression in Eq. (8) numerically, assuming that the impurity remains in the lower band. Figure 3(a) shows that the transverse conductivity of the polaron has the same sign as that of the majority particles, as given by their Chern number $\mathcal{C}$. Moreover, σ^P_{xy} vanishes when the majority particles are in a trivial phase ($\mathcal{C} = 0$). Thus, the polaron inherits the Hall-type transport properties of its dressing cloud, which is an effect solely due to interactions and which is deeply rooted in the topology of the underlying Chern insulator; this reflects the transverse drag that the majority particles impose on the impurity.

Macroscopically, one could anticipate that $\sigma^P_{xy} = 0$ whenever the majority particles are in the trivial phase (with

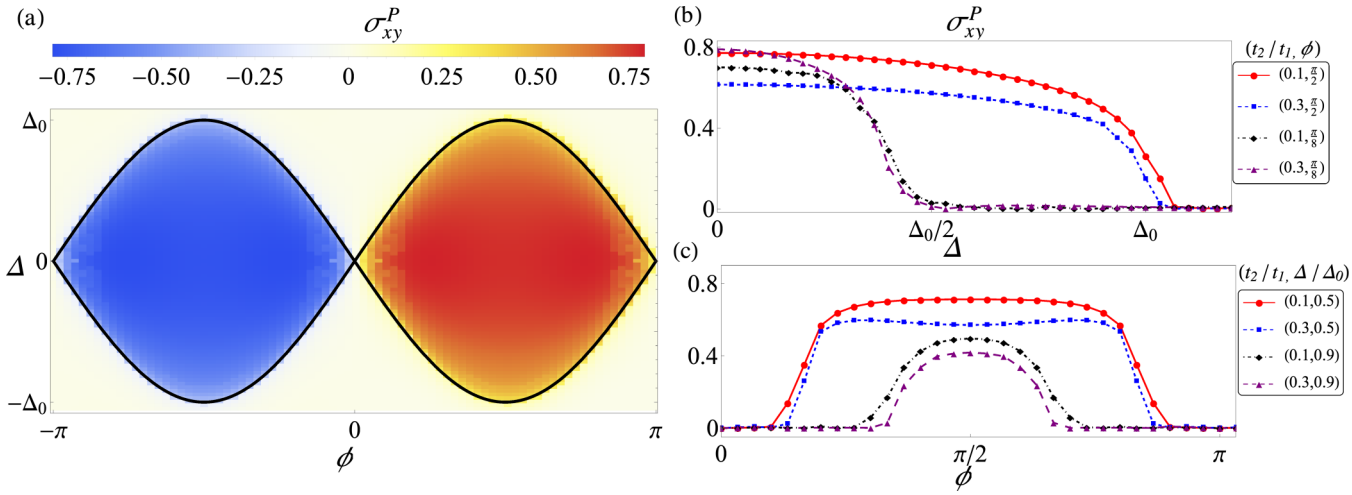

FIG. 3. (a) Transverse conductivity σ^P_{xy} of the polaron in units of g^2/Ng_0^2 with $g_0 = (2\pi a)^2/(3\sqrt{3}/2)t_1$, as a function of ϕ and Δ for $t_2 = 0.1t_1$. The solid lines give the boundaries $\Delta = \pm 3^{3/2} t_2 \sin\phi$ for the topological phase of the majority atoms. (b) and (c) depict σ^P_{xy} for fixed values of $(t_2/t_1, \phi)$ and $(t_2/t_1, \Delta/\Delta_0)$ respectively.

no net transverse current). However, this is not so obvious microscopically, as the individual majority particles exhibit a transverse motion also in the trivial phase due to the nonzero Berry curvature of the Haldane band [51,52]; since the impurity-majority scattering rate depends on the quantum states involved, this could lead to a net transverse drag on the impurity. We attribute the vanishing of σ^P_{xy} to the fact that, in the trivial phase, one can use a single gauge to describe the majority particles, and hence to the polaron eigenstates in Eq. (7).

While the transverse conductivity of the polaron is intimately related to the topological properties of its dressing cloud, it is not quantized: As shown in Figs. 3(b) and 3(c), it varies slightly as ϕ and Δ are changed, leading to a saddle-point-like surface. This reflects the composite many-body nature of the polaron, whose transport and geometric properties arise as a combination of the topological properties associated with the majority and a series of nonuniversal features

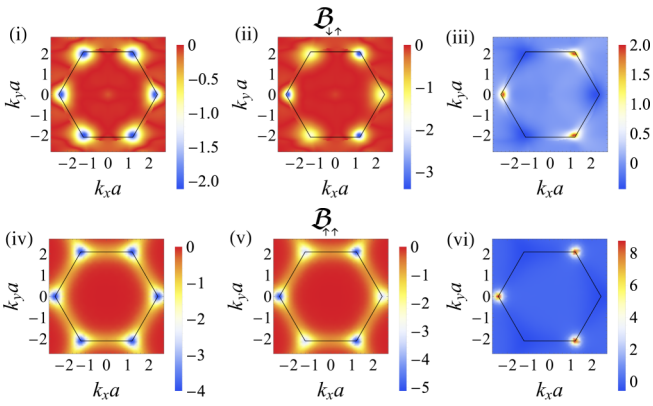

FIG. 4. (i)–(iii) The composite Berry curvature $\mathcal{B}_{\downarrow\uparrow}(\mathbf{Q})$ of the polaron for (i) $(\phi, \Delta) = (-\pi/2, 0)$, (ii) $(\phi, \Delta) = (-\pi/2, \Delta_0/3)$, and (iii) $(\phi, \Delta) = (-\pi/2, 5\Delta_0/3)$. (iv)–(vi) below show the corresponding Berry curvature $\mathcal{B}_{\uparrow\uparrow}(\mathbf{Q})$ for the majority for the same values of (ϕ, Δ).

(e.g., interactions). To further investigate the geometric properties of the polaron, we present its composite Berry curvature $\mathcal{B}_{\downarrow\uparrow}(\mathbf{Q})$, and the corresponding Berry curvature $\mathcal{B}_{\uparrow\uparrow}(\mathbf{Q})$ of the populated Haldane band in Figs. 4(i)–4(vi), for various values of (ϕ, Δ). Figures 4(i) and 4(ii) and Figs. 4(iv) and 4(v) correspond to the topological phase with $\mathcal{C} = -1$, and Figs. 4(iii) and 4(vi) correspond to the topologically trivial phase. One finds that the composite Berry curvature $\mathcal{B}_{\downarrow\uparrow}(\mathbf{Q})$ closely mimics the Berry curvature $\mathcal{B}_{\uparrow\uparrow}(\mathbf{Q})$ of the Haldane band, and that it inherits all its asymmetric features. This shows that the *geometric* properties of the Haldane model are faithfully mapped onto the polaron, at the microscopic level of the polaron wave function. We point out that the precise shape of $\mathcal{B}_{\downarrow\uparrow}(\mathbf{Q})$ differs from $\mathcal{B}_{\uparrow\uparrow}(\mathbf{Q})$, which indicates how the polaron Hall conductivity deviates from the quantized value experienced by the majority.

A nonzero temperature will reduce or smoothen the jump of the polaron's transverse conductivity at the topological transition, due to the thermal population of the excited band, but a well-defined feature should remain visible as long as the temperature is well below the band gap. To quantify more precisely this effect, our diagrammatic formalism may be extended by means of finite-temperature Green's functions.

Concluding remarks. The intricate interplay between many-body physics and topology discussed in this Rapid Communication can be studied using present cold-atom technology. Polarons have been systematically investigated by several groups [35–40]. Moreover, the Haldane model has been realized and the Berry curvature of its energy bands observed, using optical lattices [53–55]. The Hall conductivity of neutral atoms can be measured through transverse drift dynamics [56–61] or via circular dichroism [62]. We estimate the transverse velocity $v_{x\downarrow}$ of the impurity using $j_{x\downarrow} = n_\downarrow v_{x\downarrow} = \sigma^P_{xy} F_y$, where $n_\downarrow \sim 1/Na^2$ is the impurity density with a the lattice constant. From this, the transverse displacement of the impurity after time τ is $\delta x_\downarrow = \sigma^P_{xy} F_y \tau / n_\downarrow \approx 0.25(n_\uparrow g/6t_1)^2 a^2 F_y \tau$, where we have used a typical value $\sigma^P_{xy} \simeq 0.8 g^2/Ng_0^2$ (see Fig. 3). Hence,

for typical experimental times $\tau \approx 20$–$50\pi/t_1$ and $F_y \approx 0.2$–$0.3t_1/a$ [53], the transverse impurity displacement is significant, i.e., $\delta x_\downarrow \approx 1$–$5a$, even when the coupling g is small compared to the "graphene bandwidth" $6t_1$, so that our perturbative calculation is reliable. In typical polaron experiments, the concentration of impurities is typically $\lesssim 20\%$. For such concentrations, the effects of polaron-polaron interactions are negligible due to the incompressibility of the Fermi gas [38].

We showed that the transverse conductivity of the polaron scales as g^2, when the force acts on both the impurity and its dressing cloud. In fact, our result also holds when the force acts on the dressing cloud only. If instead the force acts only on the impurity, we expect the transverse conductivity to scale as g^4. First, the longitudinal motion of the impurity due to the external force induces a longitudinal drag on the majority particles, which scales with the scattering cross section $\propto g^2$. The Berry curvature of the Haldane bands will then cause a transverse drift of the majority particles [51,52], which causes a drag back on the impurity scaling with g^2, giving a total g^4 scaling. For strong coupling, we expect the transverse current to saturate when the impurity binds a single Haldane particle to form a dimer state.

Our results open up the exciting perspective of studying interacting topological systems using quantum impurities in atomic gases as a highly controllable probe.

Acknowledgments. A.C.-G. and G.M.B. acknowledge the support of the Villum Foundation. Work in Brussels was supported by the Fonds De La Recherche Scientifique (FRS-FNRS) Belgium and the ERC Starting Grant TopoCold. P.M. acknowledges the Spanish MINECO (FIS2017-84114-C2-1-P) and the "Ramón y Cajal" program.

[1] M. Z. Hasan and C. L. Kane, Rev. Mod. Phys. **82**, 3045 (2010).
[2] X.-L. Qi and S.-C. Zhang, Rev. Mod. Phys. **83**, 1057 (2011).
[3] B. Bernevig and T. Hughes, *Topological Insulators and Topological Superconductors* (Princeton University Press, Princeton, NJ, 2013).
[4] B. Bradlyn, L. Elcoro, J. Cano, M. G. Vergniory, Z. Wang, C. Felser, M. I. Aroyo, and B. A. Bernevig, Nature (London) **547**, 298 (2017).
[5] F. Schindler, A. M. Cook, M. G. Vergniory, Z. Wang, S. S. P. Parkin, B. A. Bernevig, and T. Neupert, Sci. Adv. **4**, eaat0346 (2018).
[6] F. Schindler, Z. Wang, M. G. Vergniory, A. M. Cook, A. Murani, S. Sengupta, A. Y. Kasumov, R. Deblock, S. Jeon, I. Drozdov, H. Bouchiat, S. Guéron, A. Yazdani, B. A. Bernevig, and T. Neupert, Nat. Phys. **14**, 918 (2018).
[7] A. S. Sørensen, E. Demler, and M. D. Lukin, Phys. Rev. Lett. **94**, 086803 (2005).
[8] S. Raghu, X.-L. Qi, C. Honerkamp, and S.-C. Zhang, Phys. Rev. Lett. **100**, 156401 (2008).
[9] K. Sun, H. Yao, E. Fradkin, and S. A. Kivelson, Phys. Rev. Lett. **103**, 046811 (2009).
[10] C. N. Varney, K. Sun, M. Rigol, and V. Galitski, Phys. Rev. B **82**, 115125 (2010).
[11] V. Gurarie, Phys. Rev. B **83**, 085426 (2011).
[12] C. N. Varney, K. Sun, M. Rigol, and V. Galitski, Phys. Rev. B **84**, 241105 (2011).
[13] N. R. Cooper and J. Dalibard, Phys. Rev. Lett. **110**, 185301 (2013).
[14] M. Hohenadler and F. F. Assaad, J. Phys.: Condens. Matter **25**, 143201 (2013).
[15] C. Wang, A. C. Potter, and T. Senthil, Science **343**, 629 (2014).
[16] C.-K. Chiu, J. C. Y. Teo, A. P. Schnyder, and S. Ryu, Rev. Mod. Phys. **88**, 035005 (2016).
[17] M. Calvanese Strinati, E. Cornfeld, D. Rossini, S. Barbarino, M. Dalmonte, R. Fazio, E. Sela, and L. Mazza, Phys. Rev. X **7**, 021033 (2017).
[18] C. Repellin, T. Yefsah, and A. Sterdyniak, Phys. Rev. B **96**, 161111 (2017).
[19] X.-Y. Dong, A. G. Grushin, J. Motruk, and F. Pollmann, Phys. Rev. Lett. **121**, 086401 (2018).
[20] S. Rachel, Rep. Prog. Phys. **81**, 116501 (2018).
[21] N. Goldman, J. C. Budich, and P. Zoller, Nat. Phys. **12**, 639 (2016).
[22] N. R. Cooper, J. Dalibard, and I. B. Spielman, arXiv:1803.00249.
[23] D.-W. Zhang, Y.-Q. Zhu, Y. X. Zhao, H. Yan, and S.-L. Zhu, arXiv:1810.09228.
[24] S. Rachel and K. Le Hur, Phys. Rev. B **82**, 075106 (2010).
[25] D. Cocks, P. P. Orth, S. Rachel, M. Buchhold, K. Le Hur, and W. Hofstetter, Phys. Rev. Lett. **109**, 205303 (2012).
[26] P. Kumar, T. Mertz, and W. Hofstetter, Phys. Rev. B **94**, 115161 (2016).
[27] T. I. Vanhala, T. Siro, L. Liang, M. Troyer, A. Harju, and P. Törmä, Phys. Rev. Lett. **116**, 225305 (2016).
[28] M. E. Tai, A. Lukin, M. Rispoli, R. Schittko, T. Menke, D. Borgnia, P. M. Preiss, F. Grusdt, A. M. Kaufman, and M. Greiner, Nature (London) **546**, 519 (2017).
[29] G. Salerno, M. Di Liberto, C. Menotti, and I. Carusotto, Phys. Rev. A **97**, 013637 (2018).
[30] C.-M. Jian and C. Xu, Phys. Rev. X **8**, 041030 (2018).
[31] C. Chin, R. Grimm, P. Julienne, and E. Tiesinga, Rev. Mod. Phys. **82**, 1225 (2010).
[32] I. Bloch, J. Dalibard, and W. Zwerger, Rev. Mod. Phys. **80**, 885 (2008).
[33] I. Bloch, J. Dalibard, and S. Nascimbène, Nat. Phys. **8**, 267 (2012).
[34] C. Gross and I. Bloch, Science **357**, 995 (2017).
[35] A. Schirotzek, C.-H. Wu, A. Sommer, and M. W. Zwierlein, Phys. Rev. Lett. **102**, 230402 (2009).
[36] C. Kohstall, M. Zaccanti, M. Jag, A. Trenkwalder, P. Massignan, G. M. Bruun, F. Schreck, and R. Grimm, Nature (London) **485**, 615 (2012).
[37] M. Koschorreck, D. Pertot, E. Vogt, B. Fröhlich, M. Feld, and M. Köhl, Nature (London) **485**, 619 (2012).
[38] F. Scazza, G. Valtolina, P. Massignan, A. Recati, A. Amico, A. Burchianti, C. Fort, M. Inguscio, M. Zaccanti, and G. Roati, Phys. Rev. Lett. **118**, 083602 (2017).

[39] N. B. Jørgensen, L. Wacker, K. T. Skalmstang, M. M. Parish, J. Levinsen, R. S. Christensen, G. M. Bruun, and J. J. Arlt, Phys. Rev. Lett. **117**, 055302 (2016).
[40] M.-G. Hu, M. J. Van de Graaff, D. Kedar, J. P. Corson, E. A. Cornell, and D. S. Jin, Phys. Rev. Lett. **117**, 055301 (2016).
[41] F. Grusdt, N. Y. Yao, D. Abanin, M. Fleischhauer, and E. Demler, Nat. Commun. **7**, 11994 (2016).
[42] A. H. Castro Neto, F. Guinea, N. M. R. Peres, K. S. Novoselov, and A. K. Geim, Rev. Mod. Phys. **81**, 109 (2009).
[43] F. D. M. Haldane, Phys. Rev. Lett. **61**, 2015 (1988).
[44] See Supplemental Material at http://link.aps.org/supplemental/10.1103/PhysRevB.99.081105 for further details on the explicit expressions for the current operators, the current-current correlation functions, the diagrammatic approach, and Chevy's ansatz.
[45] P. Massignan, M. Zaccanti, and G. M. Bruun, Rep. Prog. Phys. **77**, 034401 (2014).
[46] F. Chevy, Phys. Rev. A **74**, 063628 (2006).
[47] D. J. Thouless, M. Kohmoto, M. P. Nightingale, and M. den Nijs, Phys. Rev. Lett. **49**, 405 (1982).
[48] F. Grusdt, A. Shashi, D. Abanin, and E. Demler, Phys. Rev. A **90**, 063610 (2014).
[49] G. Baym and L. P. Kadanoff, Phys. Rev. **124**, 287 (1961).
[50] O. Cotlet, F. Pientka, R. Schmidt, G. Zarand, E. Demler, and A. Imamoglu, arXiv:1803.08509.
[51] D. Xiao, M.-C. Chang, and Q. Niu, Rev. Mod. Phys. **82**, 1959 (2010).
[52] R. Karplus and J. M. Luttinger, Phys. Rev. **95**, 1154 (1954).
[53] G. Jotzu, M. Messer, R. Desbuquois, M. Lebrat, T. Uehlinger, D. Greif, and T. Esslinger, Nature (London) **515**, 237 (2014).
[54] L. Duca, T. Li, M. Reitter, I. Bloch, M. Schleier-Smith, and U. Schneider, Science **347**, 288 (2015).
[55] N. Fläschner, B. S. Rem, M. Tarnowski, D. Vogel, D.-S. Lühmann, K. Sengstock, and C. Weitenberg, Science **352**, 1091 (2016).
[56] H. M. Price and N. R. Cooper, Phys. Rev. A **85**, 033620 (2012).
[57] A. Dauphin and N. Goldman, Phys. Rev. Lett. **111**, 135302 (2013).
[58] D.-L. Deng, S.-T. Wang, and L.-M. Duan, Phys. Rev. A **90**, 041601 (2014).
[59] M. Aidelsburger, M. Lohse, C. Schweizer, M. Atala, J. T. Barreiro, S. Nascimbene, N. R. Cooper, I. Bloch, and N. Goldman, Nat. Phys. **11**, 162 (2015).
[60] H. M. Price, O. Zilberberg, T. Ozawa, I. Carusotto, and N. Goldman, Phys. Rev. B **93**, 245113 (2016).
[61] R. Anderson, F. Wang, P. Xu, V. Venu, S. Trotzky, F. Chevy, and J. H. Thywissen, arXiv:1712.09965.
[62] L. Asteria, D. Thanh Tran, T. Ozawa, M. Tarnowski, B. S. Rem, N. Fläschner, K. Sengstock, N. Goldman, and C. Weitenberg, arXiv:1805.11077.